skb.se

SKB P-22-17

ISSN 1651-4416
ID 1985814
November 2022

Pre-dismantling Thermo-Hydraulic modelling of the buffer in the Prototype Repository

Daniel Malmberg
Clay Technology Lund AB

Mattias Åkesson
Svensk Kärnbränslehantering AB

Data in SKB's database can be changed for different reasons. Minor changes in SKB's database will not necessarily result in a revised report. Data revisions may also be presented as supplements, available at www.skb.se.

This report is published on www.skb.se

© 2022 Svensk Kärnbränslehantering AB

Abstract

The Prototype Repository is a full-scale field experiment simulating the KBS-3V concept for disposal of spent nuclear fuel, situated in crystalline rock at a depth of 450 m in the Äspö Hard Rock Laboratory. The Prototype Repository originally consisted of six deposition holes in which copper canisters with electrical heaters are installed inside an MX-80 bentonite buffer. The buffer was installed in the years 2001- 2003 and consisted of compacted blocks and bentonite pellets. The tunnel above the deposition holes was backfilled with a mixture of bentonite and crushed rock.

The repository was divided in two sections separated by a concrete plug. The outer section, containing two deposition holes was dismantled beginning in 2010 and the bentonite buffer sampled extensively. The inner section will be retrieved beginning in 2023, and different pre-modelling activities have been part of the planning of this operation.

In this work the hydraulic state of the buffer (e.g., degree of saturation/water content) at the time of dismantling of the inner section has been analysed using thermo-hydraulic modelling carried out with the finite-element solver CODE_BRIGHT. Models of three separate deposition holes were constructed, one of deposition hole 6 in the outer section, which was used to calibrate the model, and two of deposition holes in the inner section (deposition hole 3 and 4).

The modelling strategy, in which only the canister, bentonite buffer and a small cylindrical volume of the host rock is simulated was developed when simulating the BRIE experiment. Both in that modelling, as well as in the modelling of deposition hole 6 in this work it shows good agreement with experimental data at a relatively low numerical cost.

Sammanfattning

Prototypförvaret är ett fullskaligt fältexperiment som simulerar det så kallade KBS-3V konceptet för slutförvar av utbränt kärnbränsle. Det är placerat i kristallint berg på ett djup av 450m i Äspölaboratoriet. Experimentet bestod till en början av sex olika deponeringshål, i vilka kopparkapslar med elektriska värmare installerade inuti en buffert bestående av block och pellets gjorda av MX-80 bentonit. Kopparkapslarna och bentonitbufferten installerades 2001 – 2003 och tunneln ovanför fylldes med en blandning av bentonit och stenkross.

Fältexperimentet var uppdelat i en inre och en yttre sektion som separerades av en betongplugg i tunneln ovanför deponeringshålen. Den yttre sektionen, som bestod av två deponeringshål, bröts med början år 2010 och bentonitbufferten i deponeringshålen genomgick en omfattande provtagning. Den inre sektionen, som består av fyra deponeringshål, kommer att brytas med planerad start i januari 2023. Som del i den operationen ingår flera förmodelleringsaktiviteter, av vilken modelleringen i denna rapport utgör en del.

I det föreliggande arbetet har det hydrauliska tillståndet (vattenmättnad/vattenkvot) i bufferten vid den förväntade tiden för brytning analyserats med hjälp av fullt kopplade termiska och hydrauliska modeller. Simuleringarna har genomförts med den finita elementlösaren CODE_BRIGHT. Modeller av utvecklingen i tre separata deponeringshål har genomförts och presenteras i denna rapport: en kalibreringsmodell av deponeringshål 6 i den yttre delen och två modeller av deponeringshål i den inre sektionen (deponeringshål 3 och 4) vilka är blinda prediktioner av tillståndet vid brytning.

Modelleringsstrategin som används, i vilken enbart kapseln, bufferten och en tunn cylindrisk representation av det omgivande berget ingår utvecklades i samband med modelleringen av det så kallade BRIE experiment i Äspö. Både i den modelleringen, samt i kalibreringsmodellen i detta arbete visar modellerna mycket god överenstämmelse med brytningsdata till en förhållandevis låg numerisk ”kostnad”.

Content

1 Introduction

The Prototype Repository, located in the Äspö HRL, is a full-scale trial of the Swedish KBS-3V concept for final disposal of spent nuclear fuel. At the time of writing this report the outer section of the repository had already been dismantled and planning had started for the dismantling operation of the inner part. Predictive modelling of the state of the bentonite buffer in the deposition holes were requested by SKB. The purpose was to test the capabilities to accurately model the water uptake in deposition holes using available data from the pre-installation characterization carried out in the Prototype Repository tunnel (Rhén and Forsmark 2001, Forsmark and Rhén 2005).

To carry out the modelling the strategy developed to simulate the BRIE experiment (Malmberg and Åkesson 2018) was adopted. There, the surrounding rock is conceptualized as a thin cylindrical volume consisting of low conductivity rock matrix intersected by fractures.

In this report models of deposition hole 6 (DH6), deposition hole 4 (DH4) and deposition hole 3 (DH3) are described and the results presented. The models of DH6 were compared with dismantling data to evaluate the ability to capture the evolution in that deposition hole, while the models of DH3 and DH4 are blind predictions of the state at dismantling.

We begin by describing the experiences from previous modelling of the TH evolution in the buffer of the Prototype Repository in section 2. Thereafter, in section 3 the model setup is described and in section 4 the results are presented. Finally, in section 5 a discussion on the results and some concluding remarks are presented.

2 Experiences from the modelling and dismantling of the outer section

2.1 Modelling of outer section

A TH model of the outer section of the Prototype Repository was presented by Malmberg and Kristensson (2014). In that modelling a three-step solution strategy was adopted to avoid long computational times and numerical instability:

1) A large-scale hydraulic model prior to installation of the experiment, with an empty tunnel and deposition holes, to calibrate the rock material with respect to measured inflow,
2) large-scale uncoupled thermal and hydraulic models after installation of the experiment to determine boundary conditions for the local model; and,
3) a set of local scale, coupled thermo-hydraulic models for studying the wetting process in the buffer, from installation to excavation.

To represent the hydraulic transport properties of the rock without including a complex fracture network, the host rock was represented by a set of volumes equipped with different conductivities, calibrated by comparing simulated and measured inflows to tunnel and deposition holes. A deposition hole in the local models was embedded in a 1 m thick material with low permeability, which was intersected at different positions by identified local-inflow zones (e.g. fractures). This solution strategy allowed for the modelling and prediction of the state of the buffer at the time of dismantling.

A conclusion from that modelling was that "the uncertainties in the measured inflows to the deposition holes were too large to make a precise calibration of the rock surrounding the deposition holes" and that "the buffer wetting process was sensitive to the calibration of the rock surrounding the deposition holes" (see Svemar et al. 2016). It was therefore not possible to make predictions of the final hydraulic state in any specific part of the buffer with any accuracy. Furthermore, the uncertainties in the inflow properties of the rock gave rise to a very large span in the predicted water contents/degrees of saturation in the buffer.

2.2 Dismantling data

An extensive and detailed analysis regarding the water content and the density of the buffer was performed during the dismantling of the outer section of the Protype Repository (Johannesson 2014). These measurements showed that that the buffer had essentially reached full saturation in all parts except in the central parts of the cylinder below the canisters, and in the two cylinders above the canisters (Figure 2-1). Moreover, the distribution of the water content and the dry density in some sections in both deposition holes (DH5 and DH6) showed that the wetting and the swelling in one direction was much larger than in the opposite direction, and that this pattern was more pronounced in the upper part of the buffer. This may be correlated with the mapped fractures in the case of DH5, but this does not seem to be a likely explanation for DH6. Instead, the potential formation of conducting channels in the pellets-filled slot has been addressed in this modelling task.

2.3 Pore pressure evolution

The pore pressure in the backfill in the outer section increased fast from a low level when the drainage of the tunnel was closed in November 2004. After the drainage was opened, the pore pressure increased and a relatively constant pore pressure (of ~ 1 MPa) was measured during the second half of the operating period (Goudarzi 2021), thereby indicating that the backfill was fully saturated at the time of dismantling. This was also confirmed from the subsequent sampling and analysis. Similar trends have been measured in backfill in the inner section, although the pore pressure has stabilized at a higher level (~ 2 MPa).

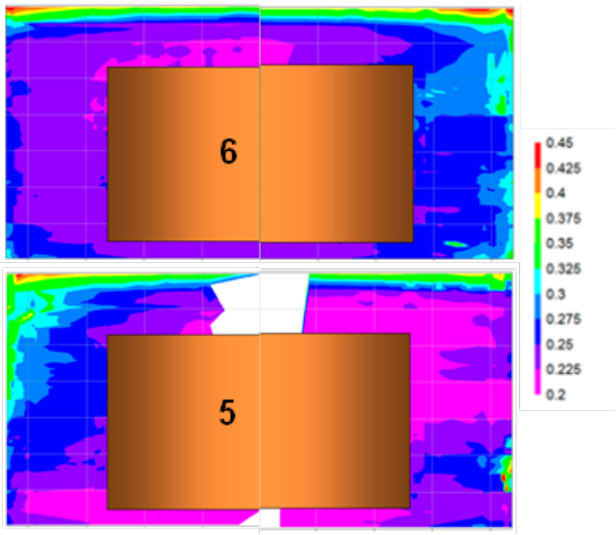

Figure 2-1: Contour plots of measured water content; composite plot for two opposite directions in deposition hole 6 (upper) and 5 (lower).

3 Model setup

The aim of the model setup was to construct a realistic conceptualisation of the properties in the field, while allowing for a relatively quick computational time. Naturally, it was necessary to include all parts of the buffer and canister, but as stated in the previous section, only a small part of the surrounding rock was simulated and the backfill above the deposition holes was not at all included in the models, except through boundary conditions.

The materials in the model were:

- Bentonite buffer (with different densities, see below)
- Copper canister
- Air gap between the buffer and canister
- Rock matrix
- Fractures

In the experiment, copper plates were placed below the bottom buffer cylinder (C1). In the models the effect of the copper plate was including by reducing the permeability of the rock below C1 by several orders of magnitude, to prevent inflow.

3.1 Dry density in the models

The models only simulated TH processes and hence changes in dry density due to swelling (a consequence of the water uptake in the bentonite) could not be directly accounted for. This has implications for both the accuracy of the modelling (as bentonite and its properties shows a strong hydro-mechanical coupling) as well as for the post-processing. For example, comparing the calculated water content in the buffer after dismantling with experimental data is difficult as the water content is not only a function of the degree of saturation, but also of the dry density. To somewhat understand the impact that the swelling and homogenization of the clay has on the results two sets of geometries were used:

- **Initial state:** The buffer components were given properties corresponding to the state just after installation in the deposition holes.
- **Final state:** The buffer was assumed to be semi-homogenized, i.e. the high density rings/cylinders had swelled, compressing the pellets column.

The properties of the buffer (e.g. dry density, dimensions etc) in the **Installation state** were taken directly from Svemar et al. (2016) while the buffer properties in the **Final state** had to be estimated from analytical models and by analysing dismantling data from the outer section. To estimate the density distribution in the final state three relations were used:

1. The mass of the block is conserved
2. The difference between the inner and the outer void ratio equals 0.15
3. The mass of block + pellets is conserved

Using these relations, it was possible to calculate the interface radius between the swollen block and compressed pellets, r_i. The interface radius calculated in this way will differ between the ring section and cylinder section. In the case of DH4 the homogenised interface radius in the ring section is 0.844 m and in the cylinder section 0.850 m. For simplicity a value of 0.850 m was used for the entire geometry. The same value of the interface radius was used in all modelled deposition holes.

3.2 Rock properties

As mentioned in section 2 above previous modelling of the Prototype Repository made use of a conceptualisation of the surrounding rock in which only a volume close to the deposition hole is well resolved, by dividing the rock into low-permeability rock matrix intersected by highly transmissive fractures. This concept, with some modifications, was also used in the modelling of the BRIE experiment in Malmberg and Åkesson (2018) and it is the experiences from those modelling exercises that have been used to construct a representation of the rock in this work.

The rock around the deposition holes was simulated as a thin cylindrical volume. The radial thickness of the rock cylinder can be estimated from the inverse of the fracture intensity (P32) from DFN models of the Prototype Repository, as described in Appendix I in Malmberg and Åkesson (2018). For the Prototype Repository the P32 value is approximately 3.41 m^2/m^3 (Stigsson et al. 2001), leading to a radial thickness of 0.3 m.

The fractures in the rock around the deposition holes were calibrated from the measured inflows during the pre-installation phase. During the calibration a liquid pressure of 0.25 MPa was prescribed on the outer surface of the rock cylinder, and a pressure of 0.1 MPa was prescribed on the wall/bottom of the deposition hole. These measurements are reported in Rhén and Forsmark (2001) and Forsmark and Rhén (2005).

In DH6 a total of 6 fractures was initially deemed necessary to include in the model. However, several of these were directly connected to the channel in the pellets (see below). As the latter was supplied with water directly from the backfill the fractures did not affect the hydraulic evolution. They did, however, cause convergence problems and in the models of DH6 presented here, they were not included. Hence, in DH6, only three fractures through the deposition hole wall and one through the bottom surface of deposition hole was simulated.

In DH4 only 1 fracture was included in the model, as no other fractures were seen in the pre-characterisation measurements. In DH3 the pre-characterisation did not detect any fracture inflows, and hence none was included in the model. The positions of the fractures are shown as the blue components in the geometry in Figure 3-1.

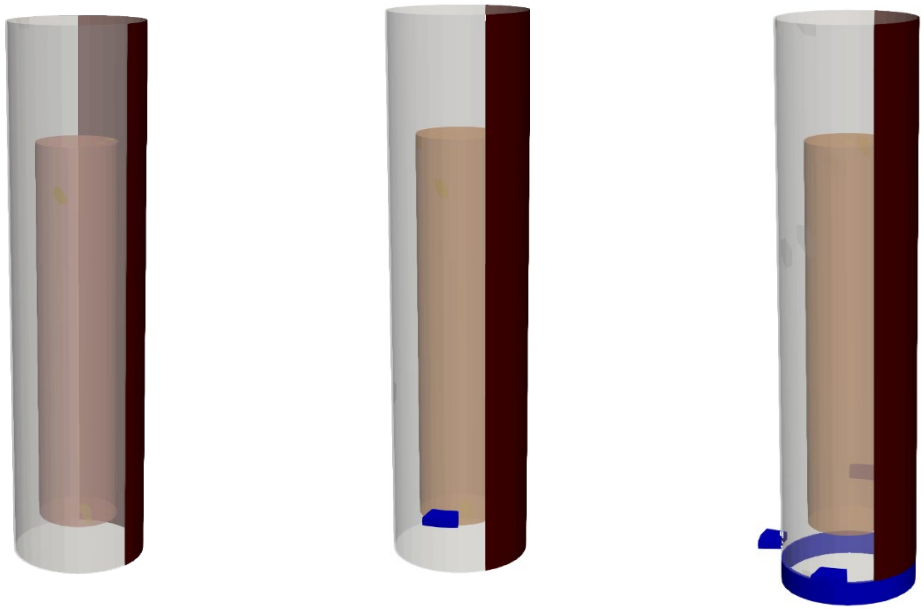

Figure 3-1. Fractures in blue and channel in the pellets in light brown as included in the geometries of DH3 (left), DH4 (middle) and DH6 (right).

3.3 Channel in the pellets

The excavation data from DH6 presented in Johannesson (2014) showed that in both DH5 and DH6 the wetting of the buffer seems to have been asymmetrical, in that one side of the buffer appears to have taken up water first and swelled, leading to a compression of the buffer/pellets on the opposite side. When constructing the models this behaviour was assumed to be due to water inflow from the backfill down through one segment of the pellet column in the deposition hole. The mechanism for the formation of such a channel in the pellet slot cannot be simulated in a TH model and hence the channel had to be directly included in the model by giving a part of the pellet slot a higher hydraulic permeability.

Although dismantling data from DH3 and DH4 was not available at the time of writing this report, it was assumed that such a preferential flow channel was formed also in these deposition holes. In DH3, data from displacement sensors do indeed suggest that the canister has been displaced in one direction by about 6 mm (Åkesson 2022).

The channel was included in the geometries as a thin slice in the outer part of the pellet slot. The orientation of the channel was selected as follows:

- DH6: Positioned on the "saturated" side of the buffer as seen in dismantling data
- DH3: Position estimated from the displacement sensors on the canister
- DH4: No data; the position in the model was taken identical to that in DH6

The channel width was assumed to be 135° of the circumferences of the deposition holes in DH6 and DH4. In DH3 a slightly narrower channel was also used (eg 112.5° and 135°) to understand the impact this may have on the evolution.

3.4 Geometry

In the initial state model, the geometry consisted of the canister, the air gap between the canister and buffer rings, the buffer rings, cylinders and pellets (with a high-permeability channel), the copper disc situated below the lower cylinder (simulated as very low-permeability rock) and the surrounding rock matrix intersected by fractures.

In the final state model, the geometry consisted of the canister, the high-density inner buffer, the low-density outer buffer (with a high-permeability channel), the copper disc below C1 (simulated as very low-permeability rock) and the surrounding rock.

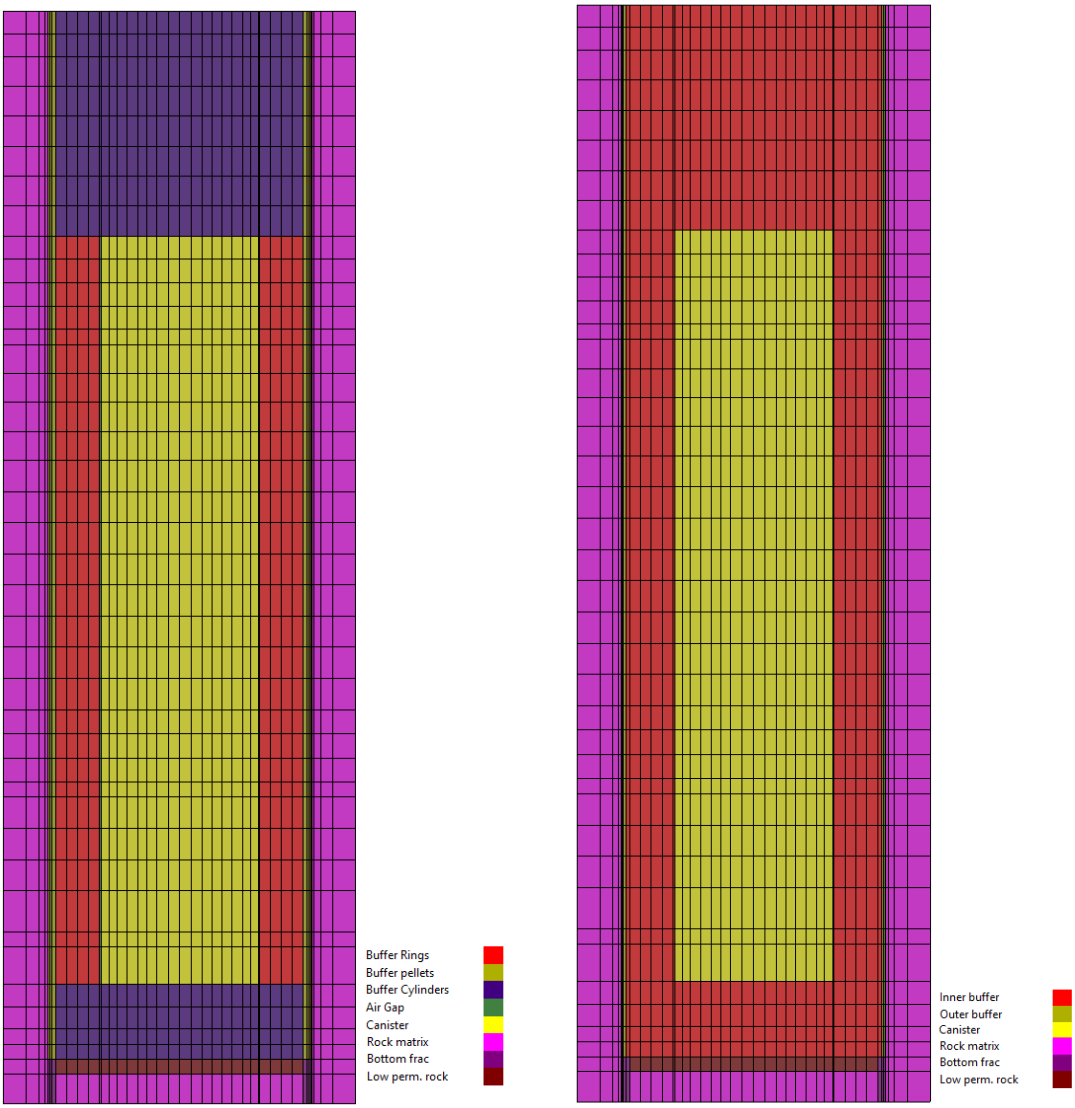

Figure 3-2. Overview of the geometry of the installation state (left) and final state (right). Not all materials are included in the picture (e.g. rock fractures). This particular geometry was used for DH6

An illustration of the two types of geometries is shown in Figure 3-2. The channel in the pellets/outer buffer and the fractures intersecting the rock matrix cannot be seen in the figure, which shows the representation used to simulated DH6.

Also seen in the figure is the mesh used in the modelling. Of particular importance is the mesh density in the rock near the interface between the rock and the buffer. The innermost elements must be small enough to sufficiently resolve the very steep liquid pressure gradient in this zone. To this effect the innermost element in the rock has a radial thickness of 0.6 cm and the next element a radial thickness of 1.6 cm in the model. This mesh density meant that the liquid pressure gradient at the rock/buffer interface is reasonable well resolved. Finer mesh densities were also attempted but proved too numerically difficult to simulate in this project.

3.5 Material parameters and initial conditions

The void ratio of the different components, as well as initial water contents, are given in Table 3-1 and material parameters are given in Table 3-2, Table 3-3 and Table 3-4. The material properties of the buffer in the installation state were taken directly from Åkesson et al. (2010) while the properties of the buffer in the homogenised state was derived using the strategy described in Åkesson et al. (2010). The relative permeability in the homogenised buffer blocks was here set to S_l^4, were S_l is the degree of saturation, in order for the moisture diffusivity of the blocks to better match experimental values.

The properties of the rock matrix were chosen from the available literature data, see Malmberg and Åkesson (2018) and references therein.

Table 3-1. Initial void ratios and water contents

	MATERIAL	VOID RATIO		WATER CONTENT
		DH3/DH4	DH6	
INSTALLATION STATE	Buffer rings	0.546	0.569	17%
	Buffer cylinders	0.610	0.623	17%
	Buffer pellets	1.78	1.78	13%
	Air gap			-
FINAL STATE MODEL	Inner buffer	0.716	0.716	17%
	Outer buffer	0.865	0.865	13%
COMMON MATERIALS	Canister	0.01[1)]		-
	Rock (matrix and fractures)	0.001		-

[1)]Unrealistically high value to simplify numerical solution.

Table 3-2. Material properties of the buffer components in the installation model

		CYLINDER	RING	PELLETS
INITIAL SUCTION	s (MPa)	46	46	100
THERMAL COND.	λ_{dry} (W/mK)	0.5	0.5	0.35
	λ_{sat} (W/mK)	1.3	1.3	1.3
SPECIFIC HEAT FOR SOLID	c (J/kgK)	800	800	800
INTRINSIC PERM.	k_0 (m^2)	$2.0 \cdot 10^{-21}$	$1.2 \cdot 10^{-21}$	$5.2 \cdot 10^{-19}$
				$1 \cdot 10^{-16}$ [1)]
	n_0 (-)	0.384	0.363	0.64
RELATIVE PERM.	k_r (-)	S_r^3	S_r^3	S_r^3
TORTUOSITY	τ (-)	0.5[2)]	0.5[2)]	0.5[2)]
RETENTION CURVE	P_0 (MPa)	43.5	67.2	0.508
	λ_0 (-)	0.38	0.48	0.26

[1)]Value for the channel in the pellets

[2)]The value was chosen from the evaluation carried out in Pintado et al. (2002). There it was shown that when using a value of 3 for the exponent in the relative permeability law a value of approx. 0.5 is suitable for the vapor diffusion tortuosity.

Table 3-3. Material properties of the non-buffer components in the models

		AIR GAP	CANISTER	ROCK	FRACTURE
INITIAL SUCTION	s (MPa)	46	46	-0.15	-0.15
THERMAL COND.	λ_{dry} (W/mK)	0.04	390	2.685	2.685
	λ_{sat} (W/mK)	0.04	390	2.685	2.685
SPEC. HEAT FOR SOLID	c (J/kgK)	1009	390	770	770
INTRINSIC PERM.	k_0 (m^2)	$1.2 \cdot 10^{-21}$	10^{-25}	$2 \cdot 10^{-20}$ [1)]	[2)]
	n_0 (-)	0.99	0.01	0.001	0.001
RELATIVE PERM.	k_r (-)	S_r^3	1	0.24[3)]	0.24[3)]
TORTUOSITY	τ (-)	1	10^{-10}	1	1
RETENTION CURVE	P_0 (MPa)	67.2	0.01	0.6	0.6
	λ_0 (-)	0.48	0.6	0.24	0.24

[1)]the permeability of the rock matrix in a 10 cm thick cylinder below C1 was set to 10^{-25} m^2 to simulate the effect of the copper plate.
[2)]The value ranges between $2x10^{-16}$ – $1x10^{-17}$ m^2 for the different fractures in the model.
[3)]van Genuchten-Mualem relation was used (DECA-UPC 2021), the value given is that of λ

Table 3-4. Material and geometrical properties of the buffer components in the final state model

		INNER BUFFER	OUTER BUFFER
INNER RADIUS	r_i (m)	-/0.525[1)]	0.85
OUTER RADIUS	r_o (m)	0.85	0.875
WATER CONTENT	w (%)	17	13
INITIAL SUCTION	s (MPa)	46	100
THERMAL CONDUCTIVITY	λ_{dry} (W/mK)	0.5	0.5
	λ_{sat} (W/mK)	1.3	1.3
SPECIFIC HEAT FOR SOLID	c (J/kgK)	800	800
INTRINSIC PERMEABILITY	k_0 (m^2)	$4.126 \cdot 10^{-21}$	$1.135 \cdot 10^{-20}$ [2)]
	n_0 (-)	0.417	0.464
RELATIVE PERMEABILITY	k_r (-)	S_r^4	S_r^4
VAPOR DIFFUSION TORTUOSITY	τ (-)	0.5[3)]	0.5[3)]
WATER RETENTION CURVE	P_0 (MPa)	7.551	3.067
	λ_0 (-)	0.18	0.20

[1)]The inner radius for the blocks around the heater was 0.525, the blocks above and below the heater were full cylinders and hence do not have an "inner radius".
[2)]In the channel material the permeability was set to $1 \cdot 10^{-16}$ m^2
[3)]The value was chosen from the evaluation carried out in Pintado et al. (2002). There it was shown that when using a value of 4 for the exponent in the relative permeability law a value of approx. 0.5 is suitable for the vapor diffusion tortuosity.

3.6 Boundary conditions

The boundary conditions to be defined are:

Thermal:

- Heat flux from the canister
- Temperature on the outer surfaces of the geometry

Hydraulic:

- Liquid pressure on the outer boundary

The power output from the canisters in DH3, DH4 and DH6 was set according to a protocol (see, for example, Goudarzi 2021) and these values were used to prescribe the heat flux in the models. Some simplifications were made, for example, by ignoring short power outages in the canisters. The prescribed heat fluxes are shown in Figure 3-3.

The boundary temperature on the outer surface of the rock was calculated analytically using the method described in Hökmark et al. (2009) by approximating all the canisters as line sources and calculating the temperature field in the surrounding rock**.** The resulting temperature was compared with temperature measurements in the rock around the Prototype Repository.

In Figure 3-4 the temperature as function of time from the analytical model is compared with the measured temperature on the deposition-hole wall around DH6, 6 meters below the tunnel floor. The analytical model slightly underestimates the measured temperature, a better fit is achieved when adding 5 °C to the curve. To calculate a boundary condition from this model the analytical equation was evaluated at the outer radius of the rock cylinder in the model, 5 °C was added to that temperature which was then prescribed on the outer wall of the geometry, as well as on the bottom surface.

In Figure 3-5 the analytically calculated temperature in one position in the rock around DH4 (black line) is shown together with the measured temperature at the same position (solid black line with squares). The agreement is good enough that the analytical calculation was just evaluated at the outer radius of the rock cylinder at the mid-height of the canister and the values prescribed as the temperature boundary condition on the outer part of the rock (red solid line).

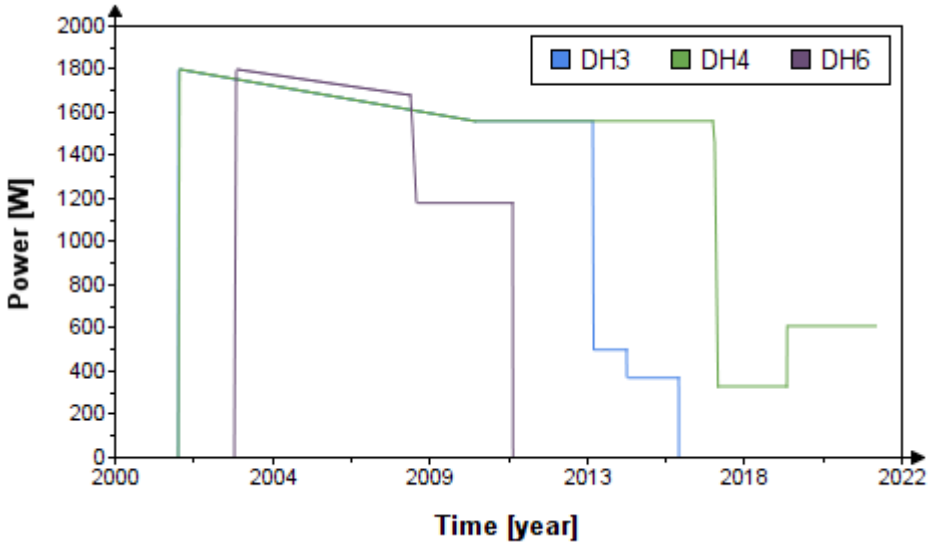

Figure 3-3. Prescribed heat flux from the canisters in DH3, DH4 and DH6

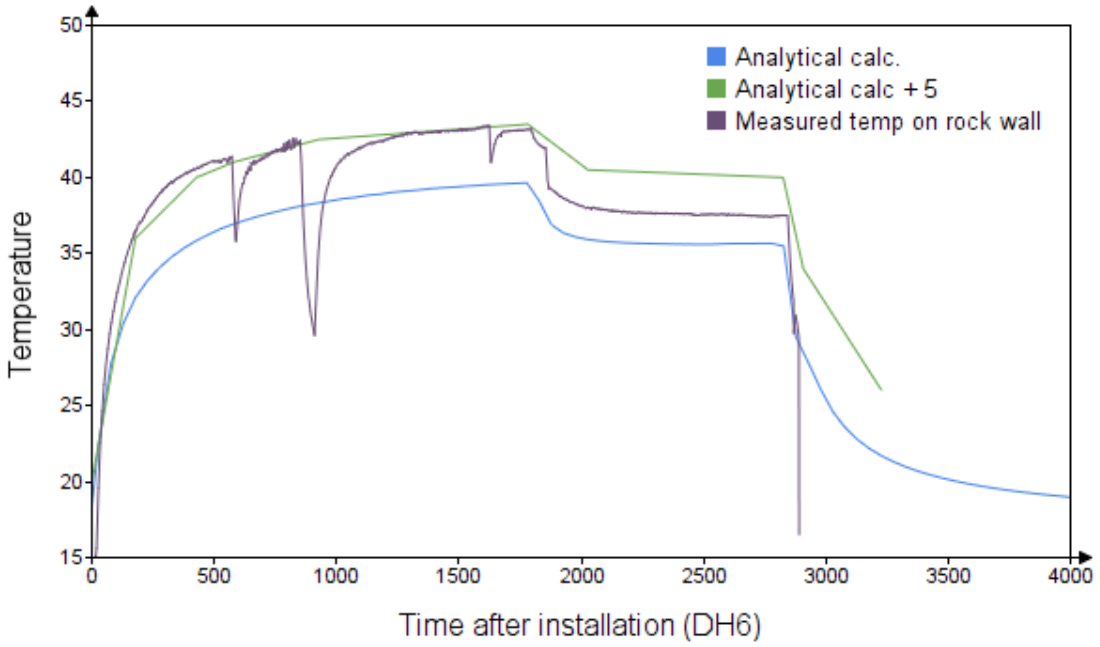

Figure 3-4. Temperature on the deposition hole wall (analytical and measured) in DH6. Comparison of the analytical calculation (blue line) with the measured temperature (purple line), shows a discrepancy which is to a large degree eliminated by adding 5 degrees C (green line).

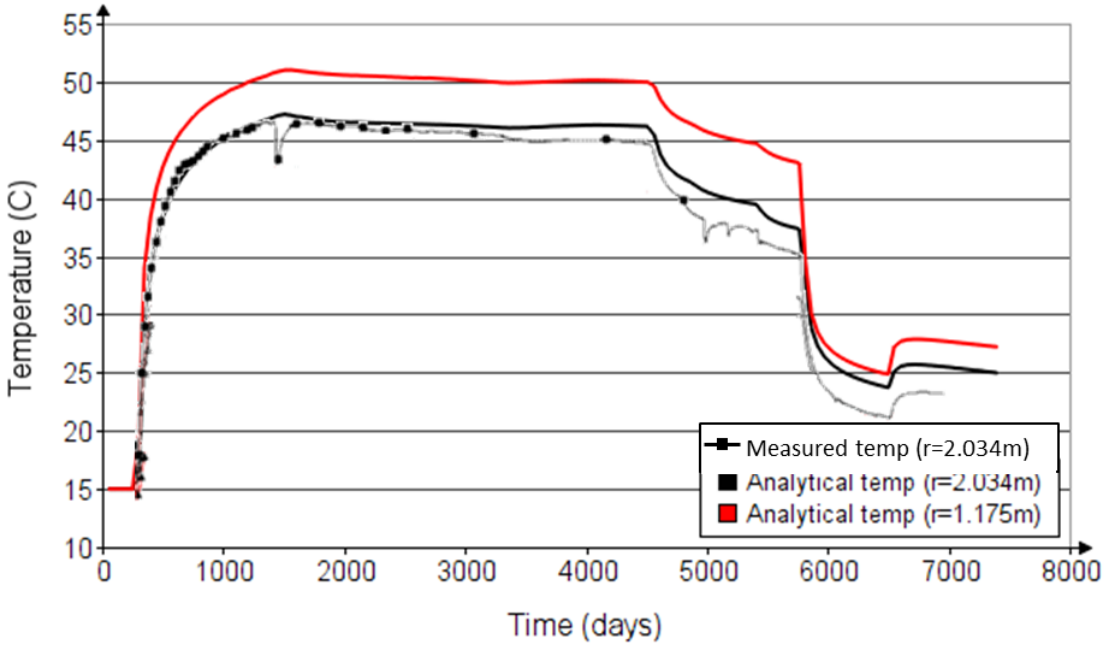

Figure 3-5. Temperature in DH4. The black solid line is the solution from the analytical calculation of the temperature field at a distance of 2.034m from the deposition hole center, and the black line with squares is the measured temperature at the same position. The red solid line corresponds to the temperature at the outer radius of the model geometry, this was used as boundary condition.

In the rock around DH3 the temperature calculated analytically is shown in Figure 3-6 as the solid thick black line. It agrees relatively well with the measured temperature at the same position (solid line with crosses. Thus, the analytical solution for the temperature was deemed good enough to use directly also here. The boundary condition applied on the outside of the rock cylinder is shown as the solid red line in Figure 3-6.

During the modelling, it was found that the temperature above the canister was overestimated in the models using these boundary conditions. To remedy this the temperature prescribed on top of cylinder 4 was decreased by 10°C, but with the condition that the prescribed temperature was never below the initial temperature of 15°C. This proved to give a good fit to the measured temperature in the buffer.

The hydraulic boundary on the outer surface of the rock cylinder, as well as on the top surface of the buffer, was prescribed from the measured pore pressure in the Prototype tunnel. Before any pore pressures were registered in the tunnel, a liquid pressure of 0.25 MPa was prescribed. The pore pressure evolution in the inner and outer sections are shown in Figure 3-7 and Figure 3-8 together with the prescribed boundary for DH3 and DH4 (inner section) as well as DH6 (outer section) respectively.

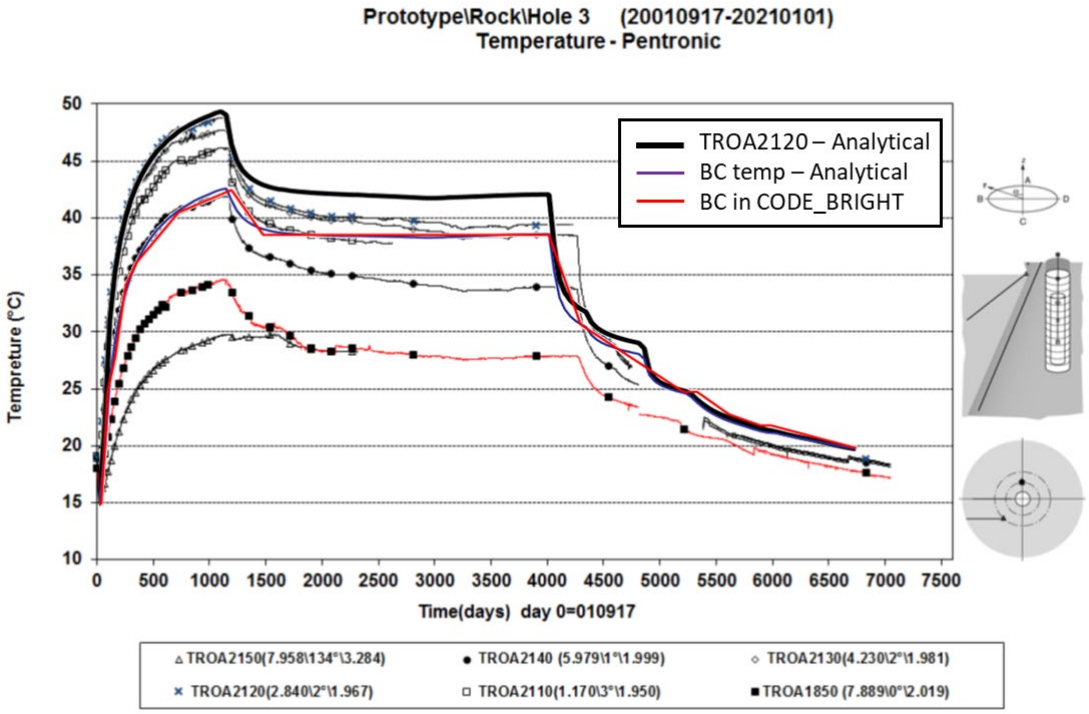

Figure 3-6. Temperature around DH3. Experimental data from Goudarzi (2021) with analytically calculated temperature in the rock (thick solid black line), analytically calculated temperature at the outer surface of the rock cylinder in the models (solid blue line) and the applied boundary condition in the model (solid red line).

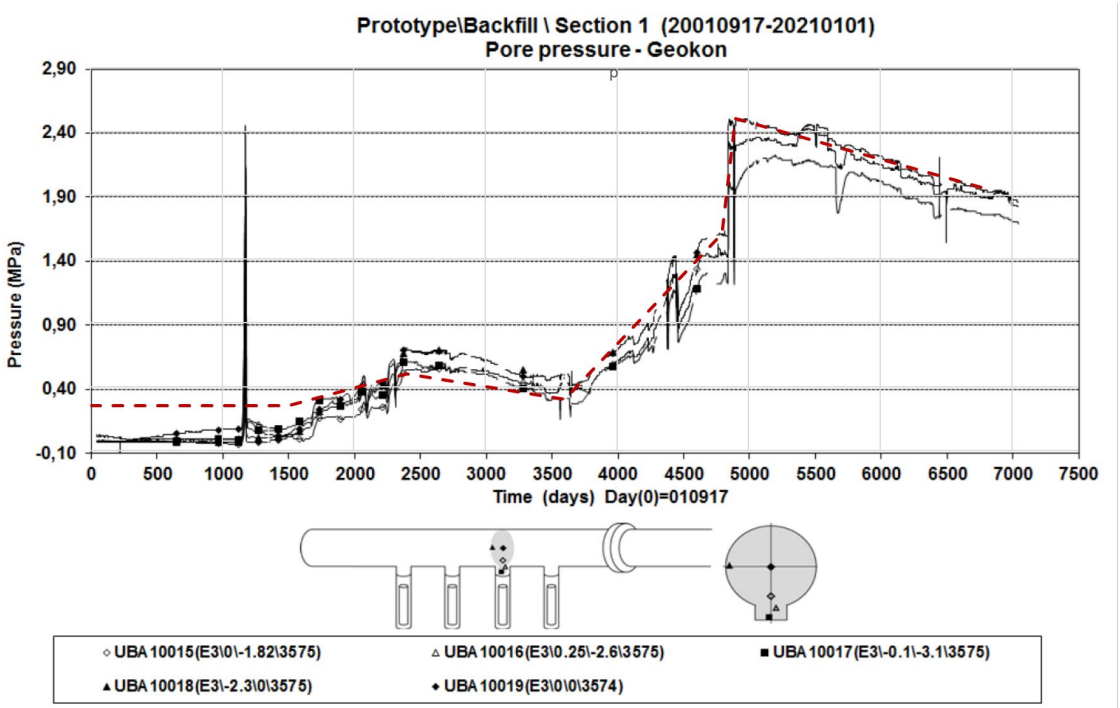

Figure 3-7. Pore pressure in the backfill in the inner section and prescribed liquid pressure (red dotted line) on the outer surfaces of the geometry in the models of DH3 and DH4.

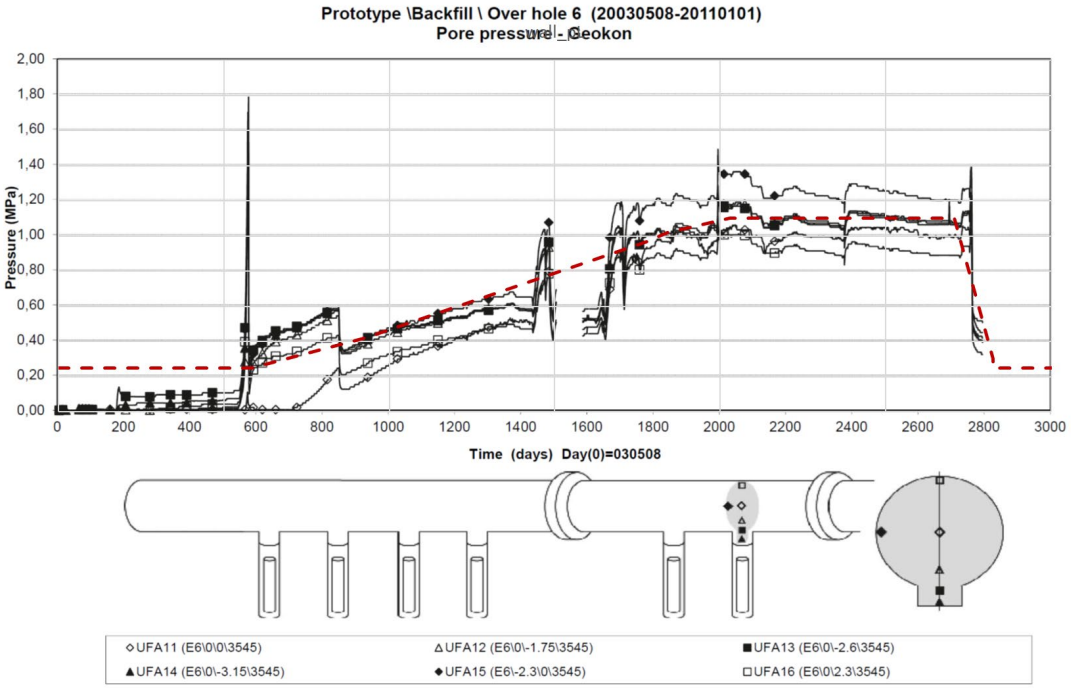

Figure 3-8. Pore pressure in the backfill in the outer section and prescribed liquid pressure (red dotted line) on the outer surfaces of the geometry in the model of DH6.

4 Results

The simulated models discussed in this report are listed in Table 4-1 with a brief description of each one. The focus of the modelling was to:

1) Determine how well the models can reproduce the final state in the already excavated DH6, and
2) Present a prediction of the state in DH3 and DH4 at the time of dismantling, which in the models was assumed to take place on the 1st of January 2023.

In this section we begin by comparing the modelled temperature evolution with sensors data from DH6 with the purpose of evaluating how well the strategy to determine the thermal boundary used here (see also section 3.6) can reproduce the thermal evolution in the field.

Thereafter a comparison between model results and field data for the hydraulic evolution is given. Unfortunately, only a few sensors have survived until the end of the operational lifetime of the repository and hence are available to compare with. In DH3 some pore pressure sensors and some RH sensors were functional, and the data from these are included below together with a comparison to model data.

After that, the final state of the models is presented and in the case of DH6 compared with dismantling data.

Table 4-1. List of models in this report

Model ID	Model name	Description
DH3_FS1	DH3_FI_M04B_V01.gid	DH3, homogenised state, channel width 135°
DH3_FS2	DH3_FI_M04_V01.gid	DH3, homogenised state, channel width 112.5°
DH4_IN	DH4_IN_M04_V01.gid	DH4, installation (initial) state, channel width 135°
DH4_FS	DH4_FI_M04_V01.gid	DH4, homogenised (final) state, channel width 135°
DH6_IN	DH6_IN_M04_V01.gid	DH6, installation (initial) state, channel width 135°
DH6_FS	DH6_FI_M04_V01.gid	DH6, homogenised (final) state, channel width 135°

4.1 Temperature evolution

As an example of the temperature evolution in the models, the evolution in the model DH6_FS is compared to experimentally measured temperatures in Figure 4-1 and Figure 4-2. As can be seen, the temperature is reasonably well reproduced in the model. The early temperature evolution around the mid-height of the canister shows a clear discrepancy with experimentally measured data, this is caused by the air gap, which is not included in this model.

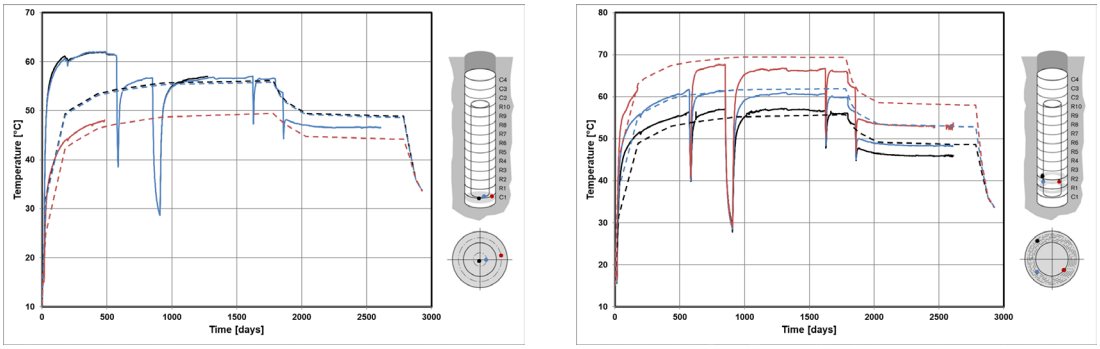

Figure 4-1. Temperature in the lower part of the buffer in DH6; solid lines represent measured data, dashed lines represent model data.

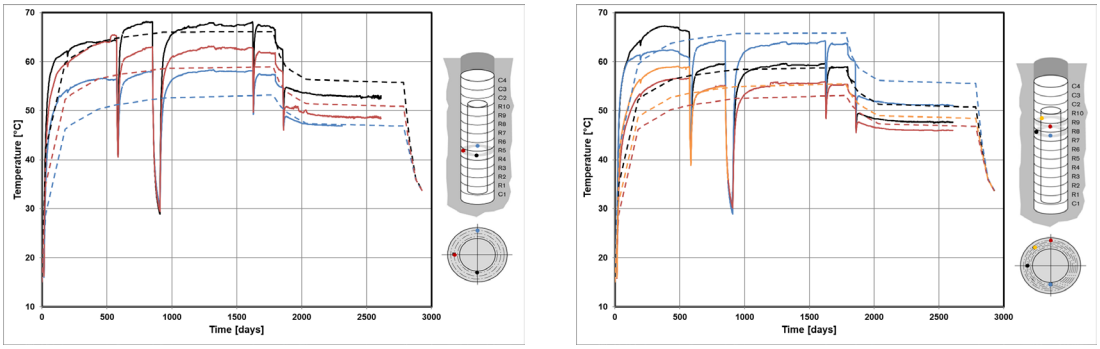

Figure 4-2. Temperature in the middle part of the buffer in DH6; solid lines represent measured data; dashed lines represent model data.

4.2 Comparison with RH/Pore Pressure sensors data

While there is no excavation data available to evaluate the models of DH3 and DH4 at the time of writing this report it can be of interest to compare the evolution in the model with sensors data. In DH4 no sensors that trace the hydraulic evolution were installed, but in DH3 both RH and pore-pressure sensors were installed, and some were still providing data late into the experiment.

In Figure 4-3 and Figure 4-4 the pore pressure evolution in DH3 is shown. The figures were taken from Goudarzi (2021). Three sensors that were still operational long into the lifetime of the project were selected (UBU30006, UBU30014, UBU300009) and compared with model data (solid lines in the figures). The point at which the pore pressure sensors start to give a value above 0 should correspond well with the time at which the buffer has reached full saturation in that point, and the model results agree relatively well in this respect. The build-up of pore-pressure after that point in general differs significantly: in the model the pore-pressure rises very quickly close to the value prescribed as a boundary condition in the model, which in turn was derived from the pore-pressure measurements in the backfill. In the sensor data the build-up is in general slower. This suggests that the applied boundary condition, with a constant pore pressure around the perimeter of the rock cylinder, is perhaps not representable of the conditions in the field. Alternatively, the slow build-up of pore pressure is due to mechanical effects, which are not captured in these TH models.

In Figure 4-5 and Figure 4-6 the RH evolution in Ring 5 and Ring 10 of DH3 is shown. The plots were taken from Goudarzi (2021). Model results at the position of sensor WBU300020 (red line in Figure 4-5) and sensor WBU30022 (blue line in Figure 4-6) have been added. As can be seen the RH evolution in Ring 5 is faster in the model, while the RH evolution in Ring 10 agrees well with experimental data.

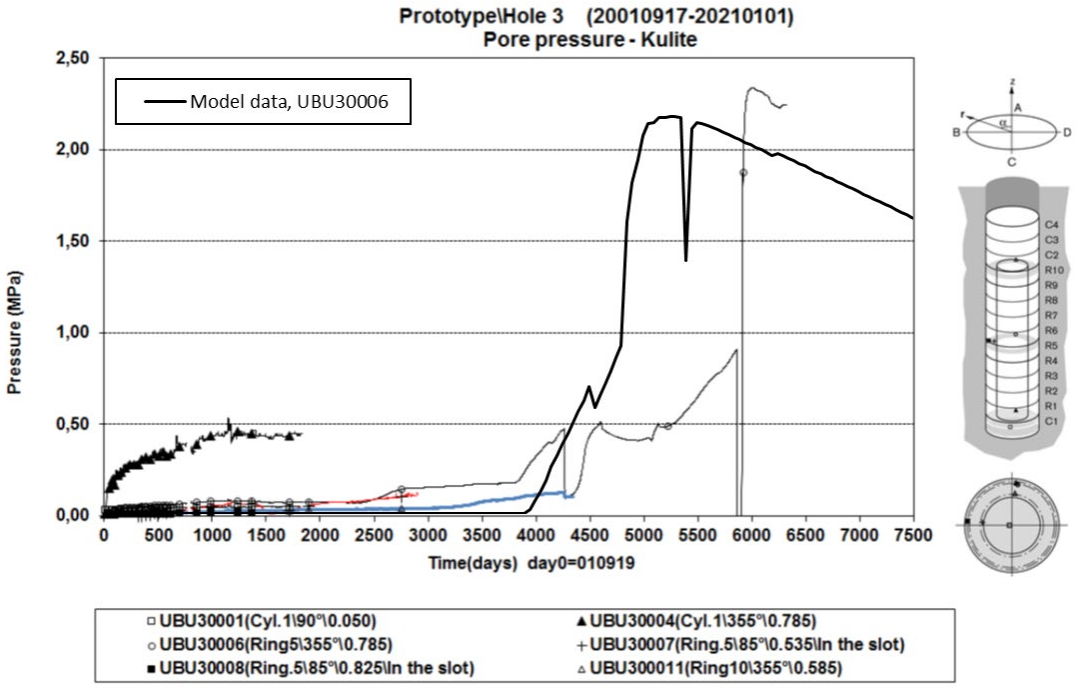

Figure 4-3. Pore pressure evolution in DH3. Figure from Goudarzi (2021) with results from the model DH3_FS2 (solid thick black line) overlayed.

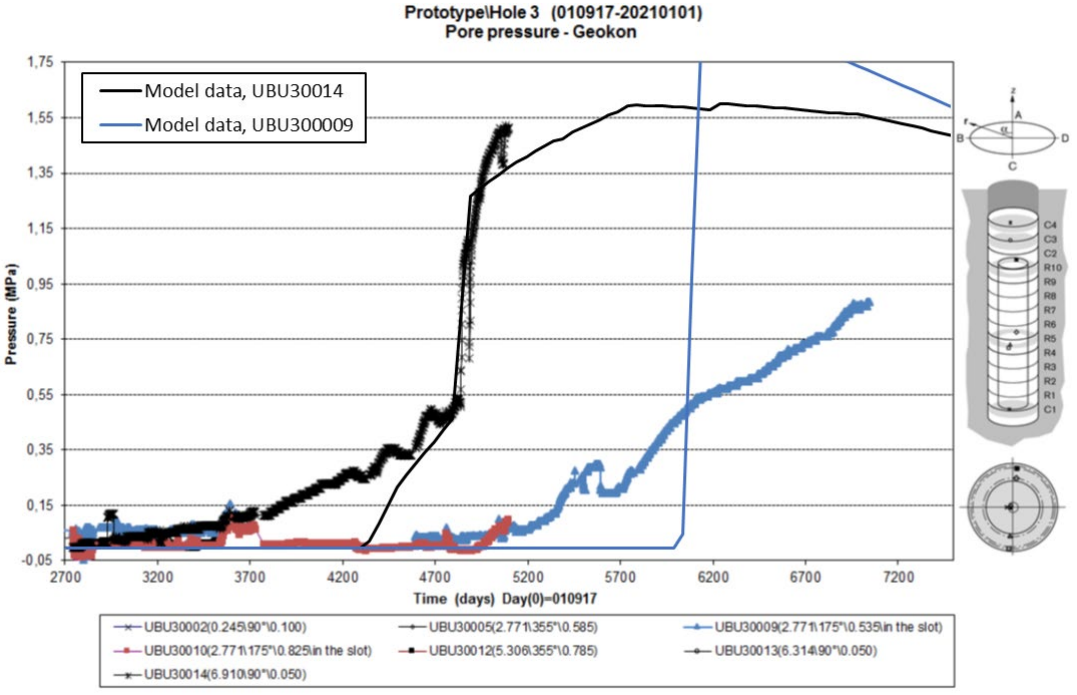

Figure 4-4. Pore pressure evolution in DH3. Figure from Goudarzi (2021) with results from the model DH3_FS2 (solid thick black and blue lines) overlayed.

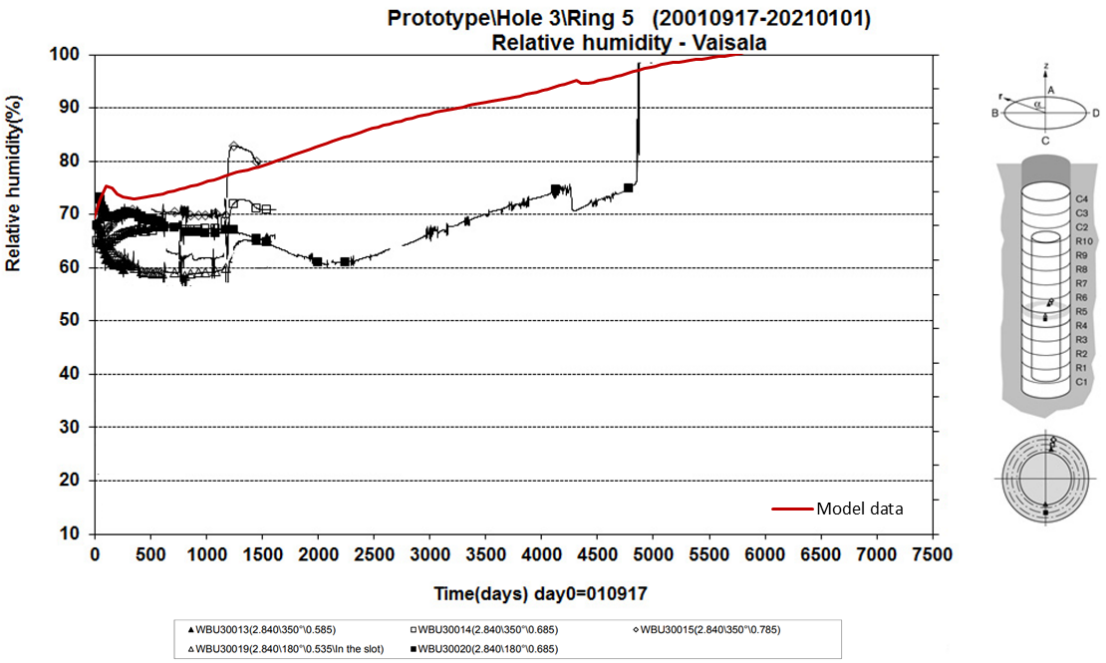

Figure 4-5 RH evolution in Ring 5 of DH3. Figure from Goudarzi (2021) with results from the model DH3_FS2 evaluated at the position of sensor WBU300020 (solid red line) overlayed.

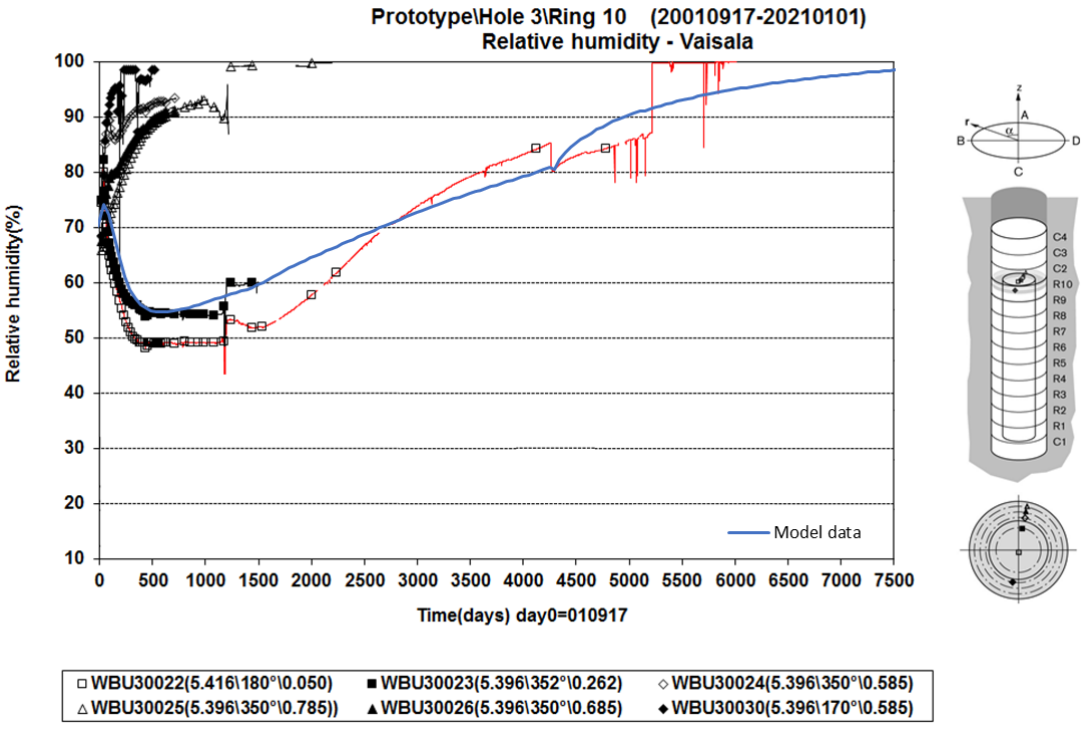

Figure 4-6. RH evolution in the field (Goudarzi 2021) with results from the model DH3_FS2 evaluated at the position of sensor WBU30022 (open squares with red solid line).

4.3 Final state in the model

The final state in the model is here evaluated as the degree of saturation and gravimetric water content at the time of dismantling. For DH6, dismantling data is available to compare with, while the results from DH3 and DH4 is a blind prediction of the expected state at dismantling.

When comparing the water content in the model with that measured in the laboratory it is important to point out that the water content is a function not only of the mass of water in the sample (given by the degree of saturation in the model) but also of the mass of solids in the volume, e.g. the dry density. In the model, the dry density is constant, and hence the water content is a function of the degree of saturation only. The adoption of a realistic dry density profile in the final state models means that these are suitable to compare with experimental water content data.

In Figure 4-7 the water content at the time of dismantling is shown from the experiment (left) and from the model of DH6 (right) with the buffer in the final semi-homogenized state (DH6_FS). The orientation of the vertical slice taken from the model was such that the right side of it intersects the middle of the channel in the pellet slot. A comparison between the model and excavation data shows that the final state in the model is rather similar to the state of the buffer in the field experiment. However, a significant difference is seen in the top part of the buffer (C3 and C4). This is to a large degree due to axial swelling, which leads to lower densities in this region of the buffer. This was not accounted for in the model and means that the water content cannot be directly compared in this region.

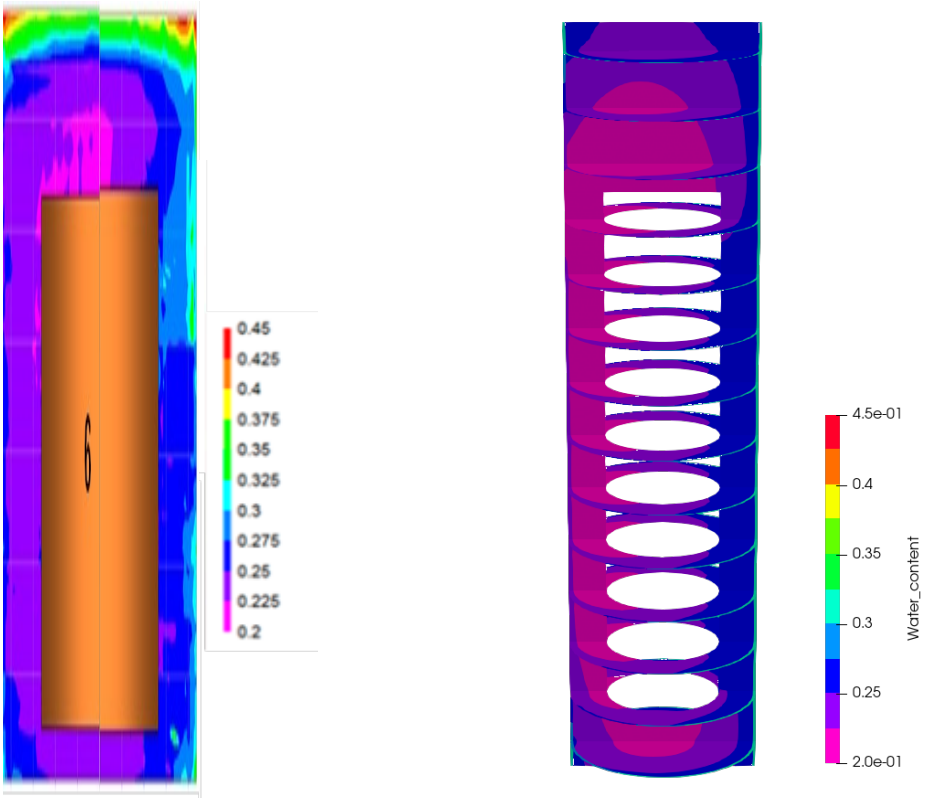

Figure 4-7. The water content at the time of dismantling from the model of DH6 with the buffer in the final semi-homogenized state (model DH6_FS, right) and excavation data to the left (Johannesson 2014).

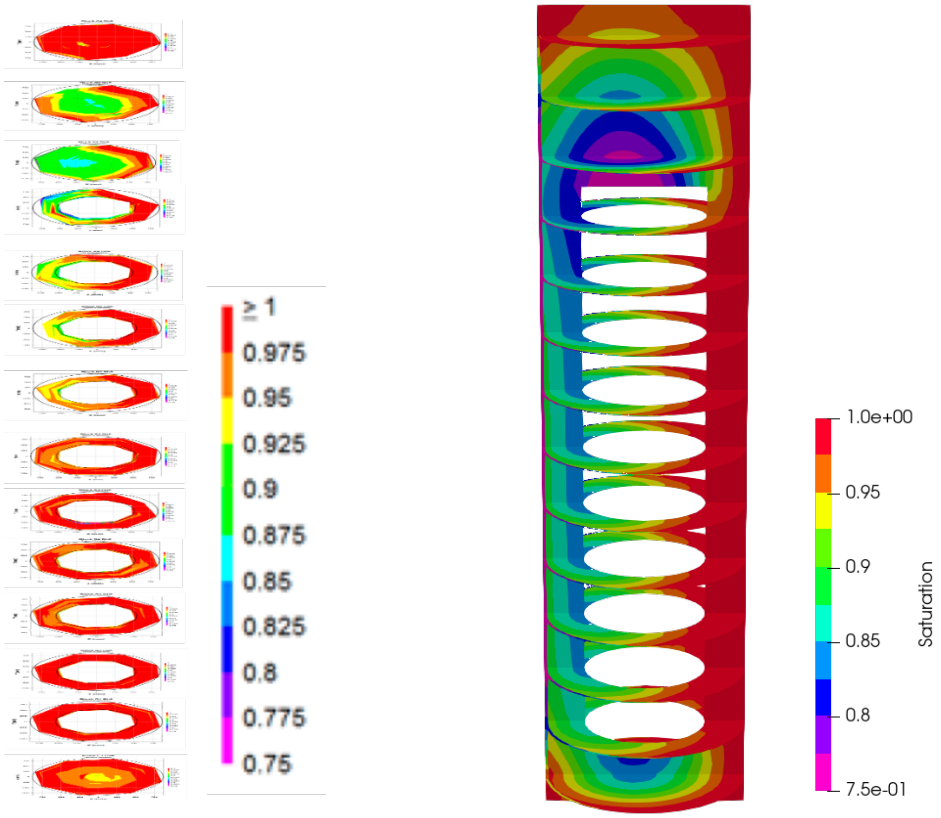

Figure 4-8. Degree of saturation at the time of dismantling from the model of DH6 (right) with the buffer in the final semi-homogenized state (from the model DH6_FS) and excavation data to the left (Johannesson 2014).

In Figure 4-8 the degree of saturation at the time of dismantling is shown from the same model together with the measured data. From this evaluation the model seems to somewhat underestimate the amount of water entering the buffer in the lower parts of the buffer, opposite of the channel in the pellet slot (lower left part of the figure). The degree of saturation in the upper part of the buffer (C3 and C4) is rather well reproduced in the model, supporting the explanation for the difference in water content seen in the same region in Figure 4-7, e.g. that the difference in the latter is due to axial swelling.

In Figure 4-9 the degree of saturation at the time of dismantling is shown from the model of DH6 with the buffer in the installation state (DH6_IN). As can be seen, this model is significantly wetter, with all the buffer rings essentially saturated. This is in line with previous modelling of the Prototype Repository (Svemar et al. 2016) – models with the buffer in the installation state tend to take up water faster than models with the buffer in the homogenised state.

It can be expected that if the mechanical evolution was simulated in the models, the results would end up somewhere in between these two results, at least if only considering the change in hydraulic permeability from the changes in dry density due to swelling/compression.

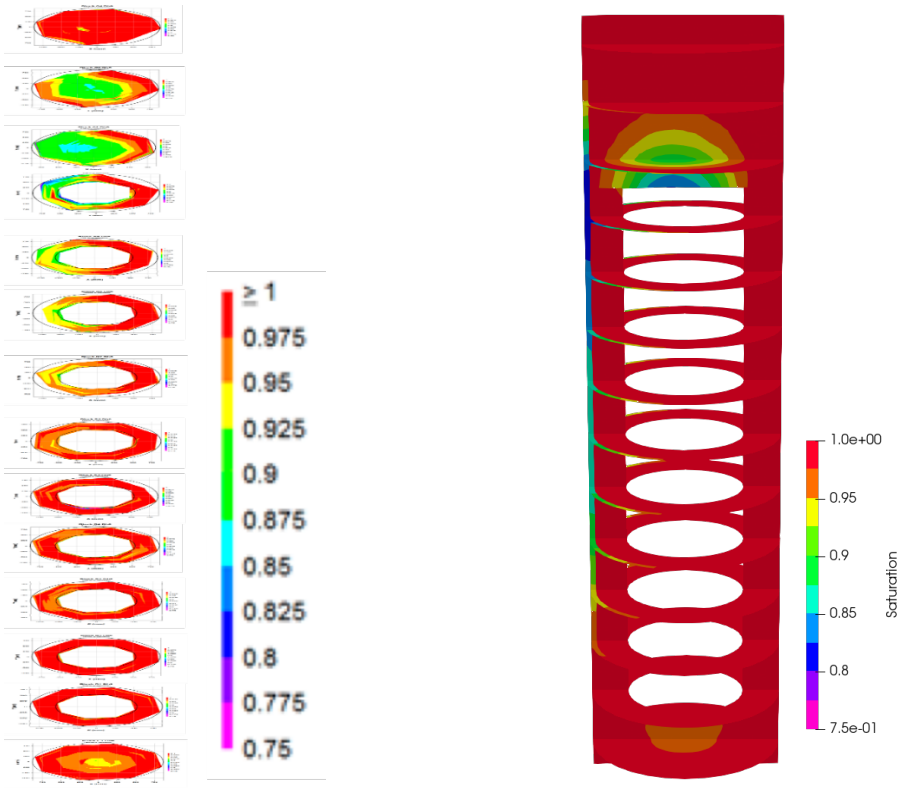

Figure 4-9. Degree of saturation at the time of dismantling from the model of DH6 with the buffer in the installation state (model DH6_IN).

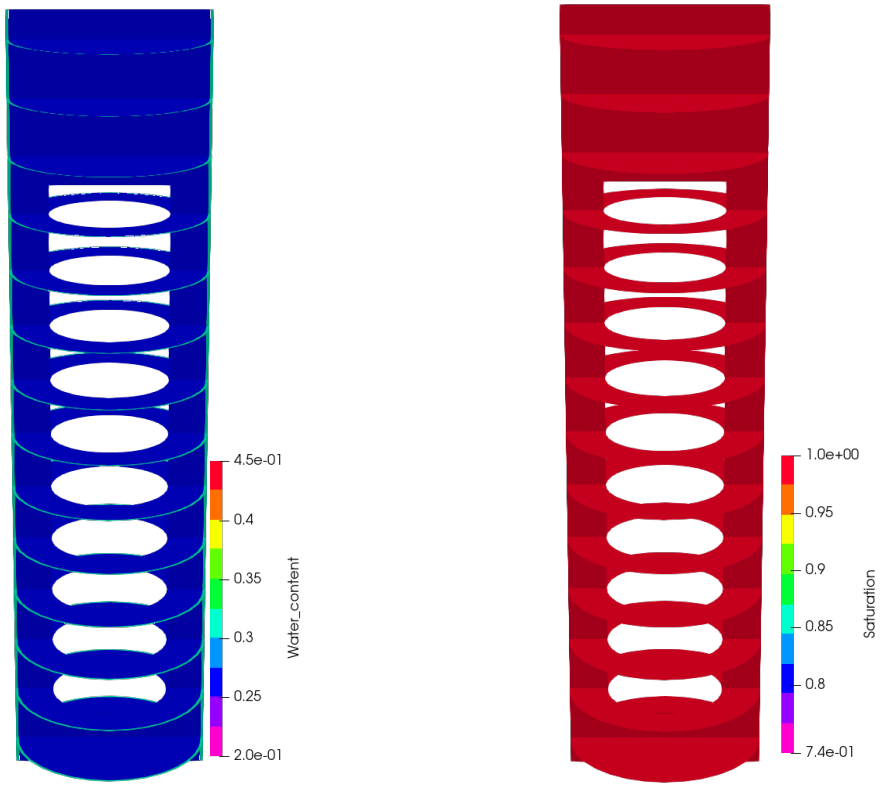

Figure 4-10. Final state in the model of DH4 with the buffer in the final semi-homogenized state (model DH4_FS). To the left is the water content at the time of dismantling, while the right plot shows the degree of saturation.

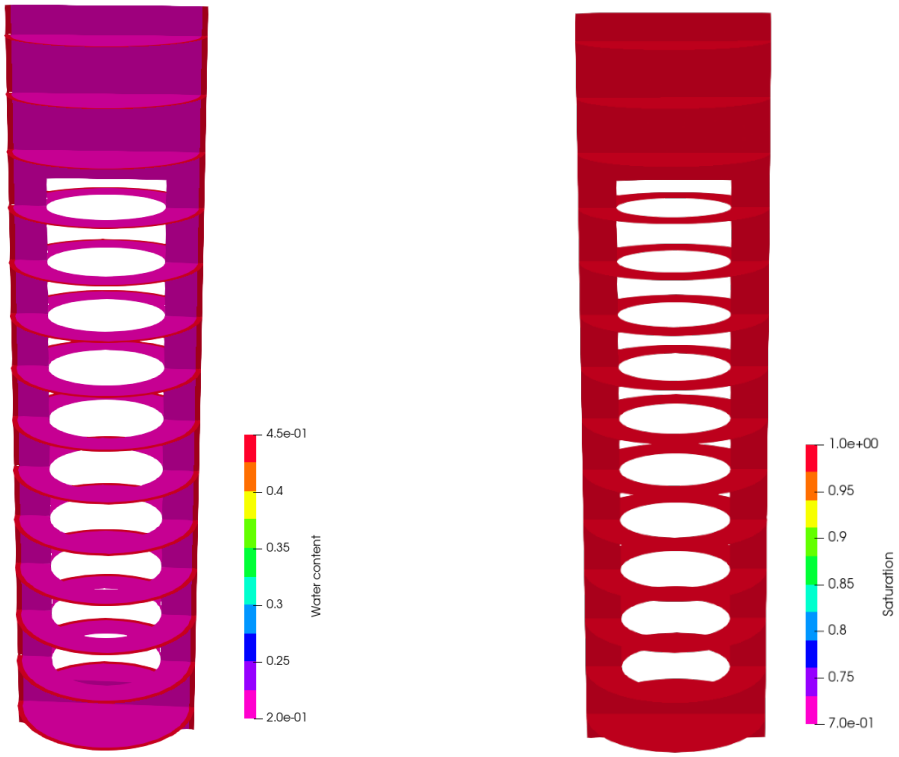

Figure 4-11. Final state in the model of DH4 with the buffer in the installation state (model DH4_IN). To the left is the water content at the time of dismantling, while the right plot shows the degree of saturation. The colour scale used to plot the water content was cut off at 0.45 to coincide with the colour scale used in Johannesson (2014). Thus, areas coloured red in the plot has a water content of $w \geq 0.45$.

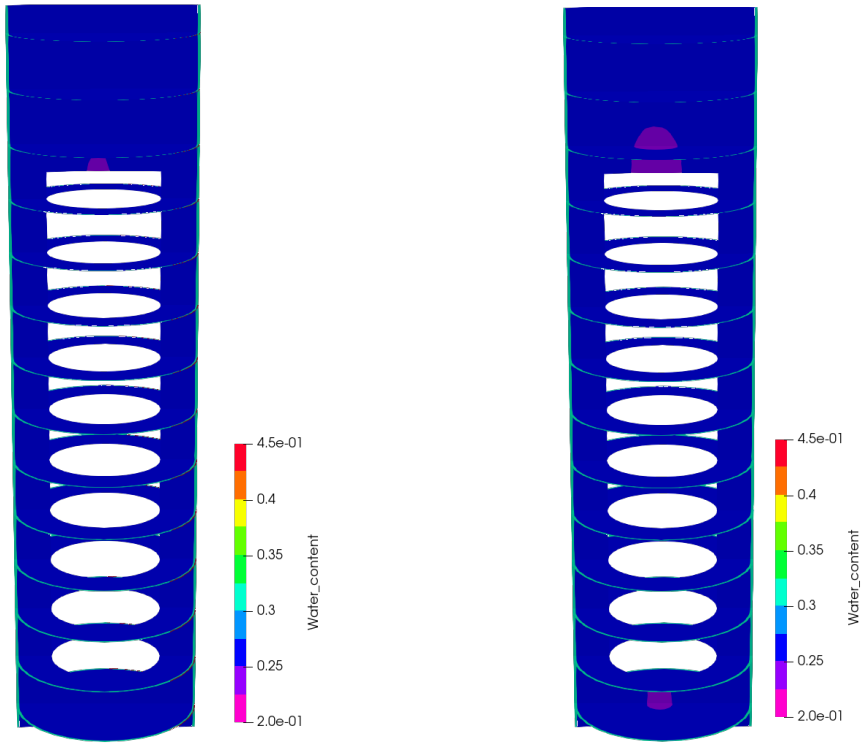

Figure 4-12. Water content at the time of expected dismantling from the model of DH3. The final state from both models is shown: DH3_FS1 (left) and DH3_FS2 (right). The difference between the two models is the width of the pellet channel.

In Figure 4-10 and Figure 4-11 the water content and degree of saturation at the expected time of dismantling (2023-01-01) is shown from the models of DH4, in the homogenised and installation states respectively. The model results suggest that the buffer in this deposition hole should be fully saturated in all points of the buffer at the time of dismantling.

During the modelling of DH3 two channel widths were used in the model (as described in section 3.3). The results from the model with the same channel width as used in the modelling of DH4 and DH6 shows that, differently from DH4 a small patch just above the canister is not fully saturated, although very close to it (see left contour plot Figure 4-12).

The model with a slightly narrower channel (112.5° vs 135°), shown in the right contour plot in Figure 4-12 shows a slightly larger unsaturated zone above the canister, and also a small patch just below.

5 Discussion and Conclusions

Models of DH3, DH4 and DH6 in the Prototype Repository has been constructed utilizing the methodology developed and used in the modelling of the BRIE experiment (Malmberg and Åkesson 2018). A similar strategy was also used in the previous modelling of the outer section of the Prototype Repository (Svemar et al. 2016).

Adding to the previously used methodology, in this modelling, data from the excavation of DH6, as well as analysis of sensors data on the canister displacement in DH3 was used to improve the model concept. This was done by assuming that water entering the deposition holes from the backfill tends to form preferential flow paths in the pellet slot around the buffer blocks, leading to asymmetric wetting from above, which can penetrate deep down into the deposition hole.

Models with such a channel was constructed and used to simulate DH6, for which excavation data is available, and DH3 and DH4. In the latter case the model results can be used as a blind prediction of the state at dismantling.

The modelling found that the buffer in DH4 is expected to be fully saturated during dismantling. In DH3 some small regions just above/below the canister may not yet have reached full saturation, although close to it, but the rest of the buffer is expected to be fully saturated.

There are several uncertainties in these predictions, in particularly related to the properties of the host rock, as well as to the formation of channels with preferential flow in the pellet slot and their properties.

5.1 Rock properties

The host rock around the prototype repository was extensively characterised before installation. However, the three different methods used (total inflow, plastic bags to collect and measure water inflow from identified inflow zones and diaper measurements) did not give a conclusive picture of the inflow properties (the inflow varied between different measurement campaigns and between the methods used) as discussed in Svemar et al. (2016). Hence, predicting the hydraulic evolution using that data alone is impossible. The models constructed and reported in Svemar et al. (2016) in general could not explain the final state in DH5 and DH6 without assuming very high matrix inflows, and when doing so the hydraulic final state was more homogeneous than what was seen during dismantling. In the modelling carried out here, the properties of the rock matrix were kept as realistic as possible and only the fractures detected in the pre-characterisation campaigns were included.

With this setup, it is necessary to assume that a significant amount of water enters the buffer in the deposition holes from the backfill to explain the dismantling data from the outer section. To capture the final state in DH6, a high permeability zone in the pellet slot had to be included to efficiently transport water from the backfill down into the deposition hole. While there is some support for that such a channel has formed in all or most of the deposition holes (see discussion in section 3.3) its properties and size is unknown and had to be guessed in the modelling presented here.

5.2 Channel formation in the pellet slot

The purpose of including a channel in the models was to explain how water may have been transported into the deposition holes according to the dismantling data from the outer section. The mechanism for how such a channel forms, and its properties and size were not considered in this work. Instead, the hydraulic properties were set identical to those in the rest of the pellet slot, except for a very high hydraulic permeability. The size of the channel was explored during the modelling, and the models discussed here, in which the channel is rather wide and extends throughout the entire depth of the deposition hole, gave the best match to dismantling data.

The two models of DH3 that were carried out, with different widths of the channel in the pellet slot showed slightly different final states, with the somewhat narrower channel giving rise to a larger (albeit still very small) unsaturated zone. Since the properties of any channels formed are highly uncertain, this creates significant uncertainties in the modelling setup.

5.3 Conclusions and future

These models have shown that with a relatively simple geometry, only including the buffer and the nearby host rock, one can successfully simulate the TH evolution in a KBS-3V deposition hole. However, large uncertainties exist which will make it difficult to predict the evolution in the planned repository without further research. For example, the inclusion of channel flow in the pellets slot was found to be very important. The likelihood for formation of such channels in the real repository (in which both lower inflows from the rock is very likely and a different tunnel backfill will be used) is highly uncertain. Previous modelling of the TH evolution in the repository (Sellin et al. 2017) showed that saturation of the deposition holes via inflows through the tunnel backfill is likely to be the dominating water transport mechanism in the repository, and hence understanding this process is important.

In the modelling carried out here inflow from the tunnel backfill proved to be a very important hydration mechanism, but in the absence of such inflows fracture and matrix inflow is of great importance. The characterisation carried out before the installation of the Prototype Repository left significant uncertainties when setting up the models to simulate the evolution, and better characterisation data would be very valuable in future field experiments.

The dismantling of the Prototype Repository will provide valuable insights into how modelling of bentonite buffers could be improved. Of particular importance for future model development would be to understand whether channels have formed in all deposition holes and what the properties of these channels were.

References

SKB's (Svensk Kärnbränslehantering AB) publications can be found at www.skb.com/publications.

DECA-UPC, 2021. CODE_BRIGHT. A 3-D program for thermo-hydro-mechanical analysis in porous media. USER'S GUIDE. Barcelona, Spain: Centro Internacional de Métodos Numéricos en Ingeniería (CIMNE).

Forsmark T, Rhén I, 2005. Äspö Hard Rock Laboratory. Prototype Repository. Hydrogeology – diaper measurements in DA3551G01 and DA3545G01, flow measurements in section II and tunnel G, past grouting activities. SKB IPR-05-03, Svensk Kärnbränslehantering AB.

Goudarzi R, 2021. Prototype Repository - Sensor data report. Period 2001-09-17 to 2020-01-01. Report No 31. SKB P-20-33, Svensk Kärnbränslehantering AB.

Hökmark H, Lönnqvist M, Kristensson O, Sundberg J, Hellström G, 2009. Strategy for thermal dimensioning of the final repository for spent nuclear fuel. SKB R-09-04, Svensk Kärnbränslehantering AB.

Johannesson L-E, 2014. Prototype Repository. Measurements of water content and density of the excavated buffer material from deposition hole 5 and 5 and the backfill in the outer section of the Prototype Repository. SKB P-13-14, Svensk Kärnbränslehantering AB.

Malmberg D, Kristensson O, 2014. Thermo-hydraulic modelling of the bentonite buffer in deposition hole 6 of the Prototype Repository. Geological Society, London, Special Publications 400, 251–263.

Malmberg D, Åkesson M, 2018. Modelling the interaction between engineered and natural barriers. Task 8 of SKB Task Forces EBS and GWFTS. SKB P-17-03, Svensk Kärnbränslehantering AB.

Pintado X, Ledesma A, Lloret A, 2002. Backanalysis of thermohydraulic bentonite properties from laboratory tests. Engineering Geology 64, 91–115.

Rhén I, Forsmark T, 2001. Äspö Hard Rock Laboratory. Prototype Repository. Hydrogeology. Summary report of investigations before the operation phase. SKB IPR-01-65, Svensk Kärnbränslehantering AB.

Sellin P (ed), Åkesson M, Kristensson O, Malmberg D, Börgesson L, Birgersson M, Dueck A, Karnland O, Hernelind J, 2017. Long re-saturation phase of a final repository. Additional supplementary information. SKB TR-17-15, Svensk Kärnbränslehantering AB.

Stigsson M, Outters N, Hermansson J, 2001. Äspö Hard Rock Laboratory. Prototype Repository. Hydraulic DFN model no:2. SKB IPR-01-39, Svensk Kärnbränslehantering AB.

Svemar C, Johannesson L-E, Grahm P, Svensson D, Kristensson O, Lönnqvist M, Nilsson U, 2016. Prototype Repository. Opening and retrieval of outer section of Prototype Repository at Äspö Hard Rock Laboratory. Summary report. SKB TR-13-22, Svensk Kärnbränslehantering AB.

Åkesson M, 2022. Prototype Repository. Estimation of the buffer homogenisation. SKB P-22-21, Svensk Kärnbränslehantering AB.

Åkesson M, Kristensson O, Börgesson L, Dueck A, Hernelind J, 2010. THM modelling of buffer, backfill and other system components. Critical processes and scenarios. SKB TR-10-11, Svensk Kärnbränslehantering AB.